

# Spectral Properties Near the Mott Transition in the One-Dimensional Hubbard Model

Masanori Kohno

*WPI Center for Materials Nanoarchitectonics, National Institute for Materials Science, Tsukuba 305-0044, Japan*

(Dated: November 22, 2018)

Single-particle spectral properties near the Mott transition in the one-dimensional Hubbard model are investigated using the dynamical density-matrix renormalization group method and the Bethe ansatz. The pseudogap, hole-pocket behavior, spectral-weight transfer, and upper Hubbard band are explained in terms of spinons, holons, antiholons, and doublons. The Mott transition is characterized by the emergence of a gapless mode whose dispersion relation extends up to the order of hopping  $t$  (spin exchange  $J$ ) in the weak (strong) interaction regime caused by infinitesimal doping.

PACS numbers: 71.30.+h, 74.72.Kf, 79.60.-i

High- $T_c$  cuprate superconductors are obtained by doping Mott insulators that have gapless spin and gapped charge excitations. Near the Mott transition, the single-particle spectral function probed by photoemission spectroscopy shows anomalous features, such as pseudogaps, Fermi arcs, hole pockets, and kinks in dispersion relations [1, 2]. It is widely believed that understanding such anomalous electronic properties near the Mott transition will be critical for achieving high- $T_c$  superconductivity.

The Mott transition can be viewed as charge localization caused by strong Coulomb repulsions; note that the nature of this transition contrasts with that of conventional metal-to-band-insulator transitions wherein a band of single-particle states is fully occupied regardless of the interactions. Further, because of the strong electronic correlations, it is generally difficult to obtain reliable information and intuitive understanding on the Mott transition. However, although some detailed properties might depend on the dimensionality of the system, it can be expected that essential features of Mott transitions are generally true for finite dimensions and that the generic features can be deduced using a one-dimensional (1D) Hubbard model. In this model, we can interpret excitations relevant to the Mott transition using exact solutions without bias. Also, we can investigate the properties of a single metallic phase all the way to the Mott transition point without causing any instability to phase separation, superconducting, or magnetic orders, which might otherwise have occurred in higher dimensions.

In this Letter, we investigate the spectral properties near the Mott transition in a 1D Hubbard chain using unbiased numerical techniques and exact solutions, focusing attention on the pseudogap, hole-pocket behavior, upper Hubbard band (UHB), and spectral-weight transfer from UHB to the lower Hubbard band (LHB). We also discuss the nature of the Mott transition through comparisons with the Fermi liquid picture and recent numerical results on the two-dimensional (2D) Hubbard model [3].

*Model and method.*— We consider the 1D repulsive Hubbard model defined by the following Hamiltonian:

$$\mathcal{H} = -t \sum_{i=1}^L \sum_{\sigma=\uparrow,\downarrow} \left( c_{i+1\sigma}^\dagger c_{i\sigma} + c_{i\sigma}^\dagger c_{i+1\sigma} \right)$$

$$+ U \sum_{i=1}^L n_{i\uparrow} n_{i\downarrow} - \mu \sum_{i=1}^L (n_{i\uparrow} + n_{i\downarrow}).$$

Here, hopping integral  $t$  and on-site repulsion  $U$  are positive. We denote the annihilation and number operators of an electron at site  $i$  with spin  $\sigma$  as  $c_{i\sigma}$  and  $n_{i\sigma}$ , respectively. The number of sites, electrons, and down spins is denoted by  $L$ ,  $N$ , and  $M$ , respectively. The doping concentration is defined as  $\delta = 1 - N/L$ . Also, we define the single-particle spectral function as follows:

$$A(k, \omega > 0) = \sum_l |\langle l | c_{k\uparrow}^\dagger | GS \rangle|^2 \delta(\omega - E_l + E_{GS}),$$

$$A(k, \omega < 0) = \sum_l |\langle l | c_{k\downarrow} | GS \rangle|^2 \delta(\omega + E_l - E_{GS}).$$

Here,  $|GS\rangle$  and  $|l\rangle$  denote the ground state with energy  $E_{GS}$  and the excited state with  $E_l$ , respectively, while  $c_{k\sigma}^\dagger$  creates an electron with momentum  $k$  and spin  $\sigma$ .

I calculated  $A(k, \omega)$  using the dynamical density-matrix renormalization group (DDMRG) method [4] under the open boundary condition with the number of density-matrix eigenstates  $m = 120$ . The data with Lorentzian broadening with half-width at half-maximum  $\eta = 0.16t$  were deconvolved to those of Gaussian broadening with standard deviation  $\sigma = 0.1t$ . The spectral functions with  $k = \pi j/(L+1)$  for  $j = 1 \sim L$  were extrapolated to  $k=0$  and  $\pi$ . Figure 1 (a) shows the typical behavior of  $A(k, \omega)$ . Since the difference between the results for  $L = 60$  and  $80$  is small in this scale, this Letter shows the results for  $L = 60$  unless otherwise mentioned. Noting that  $A(k, \omega) = A(-k, \omega) = A(k + 2\pi, \omega)$ , we consider the properties of  $0 \leq k \leq \pi$  without loss of generality.

To identify the dominant modes in  $A(k, \omega)$ , we use the Bethe ansatz. In the Bethe ansatz, the wavefunctions, energies, and momenta of eigenstates are expressed in terms of  $\{k_j\}$  and  $\{\Lambda_\alpha\}$  that satisfy the following Bethe equations [5]:  $Lk_j = 2\pi I_j + 2 \sum_{\alpha=1}^M \tan^{-1} \frac{4t(\Lambda_\alpha - \sin k_j)}{U}$  for  $j = 1 \sim N$ , and  $\sum_{j=1}^N \tan^{-1} \frac{4t(\Lambda_\alpha - \sin k_j)}{U} = \pi J_\alpha + \sum_{\beta=1}^M \tan^{-1} \frac{2t(\Lambda_\alpha - \Lambda_\beta)}{U}$  for  $\alpha = 1 \sim M$ , where  $I_j$  and  $J_\alpha$  are integers or half-odd integers depending on the values of  $N$  and  $M$ . We impose the (anti-)periodic boundary condition, when  $M$  in the ground state is odd (even). Because eigenstates are obtained through the Bethe equations using  $\{I_j\}$  and  $\{J_\alpha\}$ , the  $\{I_j\}$  and  $\{J_\alpha\}$  distributions characterize eigenstates. In the ground state,  $\{I_j\}$

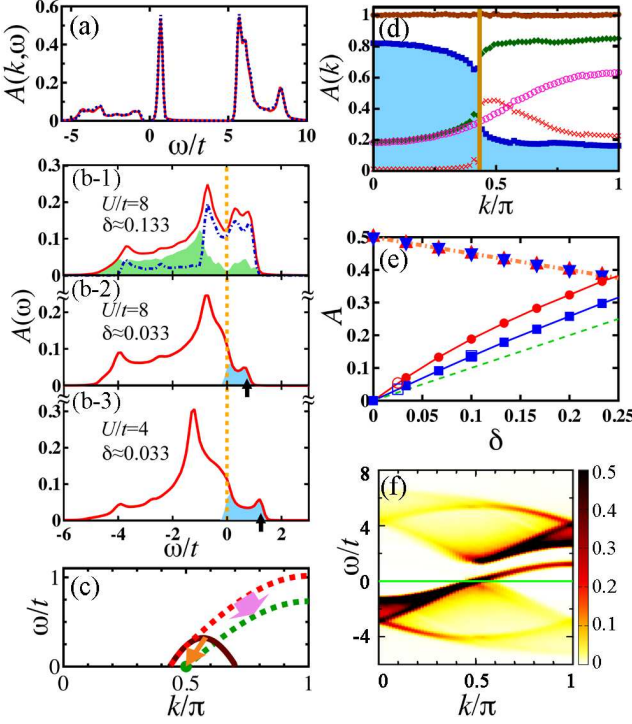


FIG. 1: (a)  $A(k, \omega)$  for  $L=60$  (red solid line) and  $80$  (blue dotted line) at  $k \approx 0.8\pi$  for  $U/t=8$  when  $\delta=0.1$ . (b)  $A(\omega)$  in the lower Hubbard band (LHB) (red lines) for (b-1)  $U/t=8$ ,  $\delta \approx 0.133$ ; (b-2)  $U/t=8$ ,  $\delta \approx 0.033$ ; and (b-3)  $U/t=4$ ,  $\delta \approx 0.033$ . In (b-1), the blue dashed-dotted line denotes the contribution of dominant modes, while the green region shows the contribution of continua except the dominant modes. In (b-2,3), the light blue regions denote the contribution from  $\omega>0$ . Arrows indicate  $\epsilon(k=\pi)$  of Eq. (1). (c) Dispersion relations of the upper edge of the  $sh^*$  continuum (red dotted line) and the  $h^*$  mode with  $s(k_F)$  (brown solid line) for  $U/t=8$  at  $\delta \approx 0.133$ . The green dotted line and the dot at  $k=0.5\pi$  show those of  $\delta \rightarrow 0$ . (d)  $A(k)=\int d\omega A(k, \omega)$  for  $U/t=8$  at  $\delta \approx 0.133$ . Blue squares with the light blue region denote the contribution from  $\omega<0$ , which is the momentum distribution function in the ground state  $n(k)$ . Green diamonds denote the contribution from  $\omega>0$ ; red crosses and pink open circles denote that of LHB for  $\omega>0$  and that of the upper Hubbard band. The vertical yellow line indicates  $k=k_F$ . Brown solid circles denote the total weight at each  $k$ , which satisfies the sum rule within numerical accuracy. (e) Doping dependence of spectral weight  $A$ . Solid lines show  $A$  of LHB for  $\omega>0$  at  $U/t=4$  (red circles) and  $8$  (blue squares). Red and blue triangles denote  $A$  for  $\omega<0$  at  $U/t=4$  and  $8$ . The green dashed line and orange dashed-dotted line indicate  $A=\delta$  and  $(1-\delta)/2$ . Open symbols denote data for  $L=80$ . (f)  $A(k, \omega)$  for  $U/t=4$  at  $\delta \approx 0.033$ .

and  $\{J_\alpha\}$  are consecutively distributed around zero. Excited states are obtained by creating holes (particles) inside (outside) the consecutive distributions of the ground state. The holes in the  $\{J_\alpha\}$  distributions are called spinons, while those in the  $\{I_j\}$  distributions are called holons. The particles created outside the consecutive distribution of  $\{I_j\}$  are called antiholons. Hereafter, we use the following shorthand notations for the spinon,

holon, and antiholon— $s$ ,  $h$ , and  $h^*$ , respectively. Noting that the momentum of the eigenstate is given by  $K = 2\pi(\sum_j I_j + \sum_\alpha J_\alpha)/L$ , we define the momenta of  $s$ ,  $h$ , and  $h^*$  as  $q_s = 2\pi J_s/L$ ,  $q_h = 2\pi I_h/L$ , and  $q_{h^*} = 2\pi I_{h^*}/L$ , respectively, where  $J_s$ ,  $I_h$ , and  $I_{h^*}$  are the positions of  $s$ ,  $h$ , and  $h^*$  in the distributions of  $\{J_\alpha\}$  and  $\{I_j\}$ . The momentum ranges are  $|q_s| < k_F$ ,  $|q_h| < 2k_F$ , and  $2k_F < |q_{h^*}| < \pi$  with the Fermi momentum  $k_F = \pi N/(2L) = \pi(1-\delta)/2$ .

*Dominant modes for  $\omega < 0$ .*— Before discussing the Mott transition, we review the dominant modes for  $\omega < 0$  at  $\delta = 0.4$  [6, 7]. The dominant mode for  $k < k_F = 0.3\pi$  near  $\omega \lesssim 0$  in Fig. 2 (a-1) is identified as the  $s$  mode without  $h$  and  $h^*$  [blue dashed-dotted line for  $k < k_F$  in Fig. 2(c-1)]. The mode slightly below it is identified as the  $h$  mode with  $s$  having  $q_s = k_F$  and  $h^*$  having  $q_{h^*} = 2k_F$ . Hereafter, we denote it as the  $h$  mode with  $s(k_F)$  and  $h^*(2k_F)$ . The mode for  $k < 3k_F = 0.9\pi$  is identified as the  $h$  mode with  $s(-k_F)$  and  $h^*(-2k_F)$ , which is called the shadow band [8]. The lower edge of the  $sh^*$  continuum is indicated by the lowest pink dotted line in Fig. 2(c-1). For  $\omega \gtrsim 0$ ,  $sh^*$  excitations are dominant [7, 9].

*Pseudogap.*— As shown by the red line in Fig. 1(b-1), the momentum-integrated spectral weight [ $A(\omega) = \int_{-\pi}^{\pi} \frac{dk}{2\pi} A(k, \omega)$ ] shows reductions near  $\omega \simeq 0$ . This pseudogap behavior originates from the following three properties: (1) low-energy property as a Tomonaga-Luttinger (TL) liquid [10, 11], (2) the band-edge singularity of the 1D dominant modes, and (3) continua spread above and below  $\omega = 0$ . In a TL liquid,  $A(\omega) \propto |\omega|^\theta$  for  $\omega \rightarrow 0$  with the same exponent as that of the momentum distribution function  $n(k) - 1/2 \propto |k - k_F|^\theta$  for  $k \rightarrow k_F$ , where  $0 < \theta < 1/8$  depending on the values of  $U/t$  and  $\delta$  [Fig. 1(d)] [10]. Because  $\theta \rightarrow 1/8$  as  $\delta \rightarrow 0$ , the pseudogap behavior will be significant near the Mott transition. Next, we extract the contribution of dominant modes by Gaussian fitting of the peaks in  $A(k, \omega)$  at each  $k$ . The contribution is shown by the blue dashed-dotted line in Fig. 1(b-1). The peaks in  $A(\omega)$  are located near the bottom of the  $s$  mode for  $\omega \lesssim 0$  and the top of the  $h^*$  mode with  $s(k_F)$  [brown solid line near  $k \simeq \pi/2$  in Fig. 2(c-2)] for  $\omega \gtrsim 0$ ; this implies that the pseudogap behavior can be explained as a dip between the peaks near the band edges of the 1D dominant modes. Moreover, the contribution from continua except the dominant modes shows reductions near  $\omega \simeq 0$ , as shown by the green region in Fig. 1(b-1). As in Fig. 2(b-2), the continua above and below  $\omega = 0$  shrink to the gapless points at  $k = k_F$  and  $2\pi - 3k_F$  as  $\omega \rightarrow 0$ . The continua for  $\omega \gtrsim 0$  are mainly due to the 2- $\Lambda$ -string solutions where two  $\Lambda_\alpha$ 's are  $\bar{\Lambda} \pm iU/(4t)$  with real  $\bar{\Lambda}$  [12] for  $k \lesssim k_F$ ,  $sh^*$  for  $k \simeq 2\pi - 3k_F$ , and  $hh^*$  excitations with  $s(k_F)$  and  $h^*(\pm 2k_F)$  for  $k \simeq 2\pi - 3k_F$  and  $k_F$ . For  $\omega \lesssim 0$ , the continua mainly come from the  $sh$  excitations with  $h^*(\pm 2k_F)$ .

*Hole-pocket behavior.*— The mode connecting the two gapless points at  $k = k_F$  and  $2\pi - 3k_F$  for  $\omega \gtrsim 0$  is

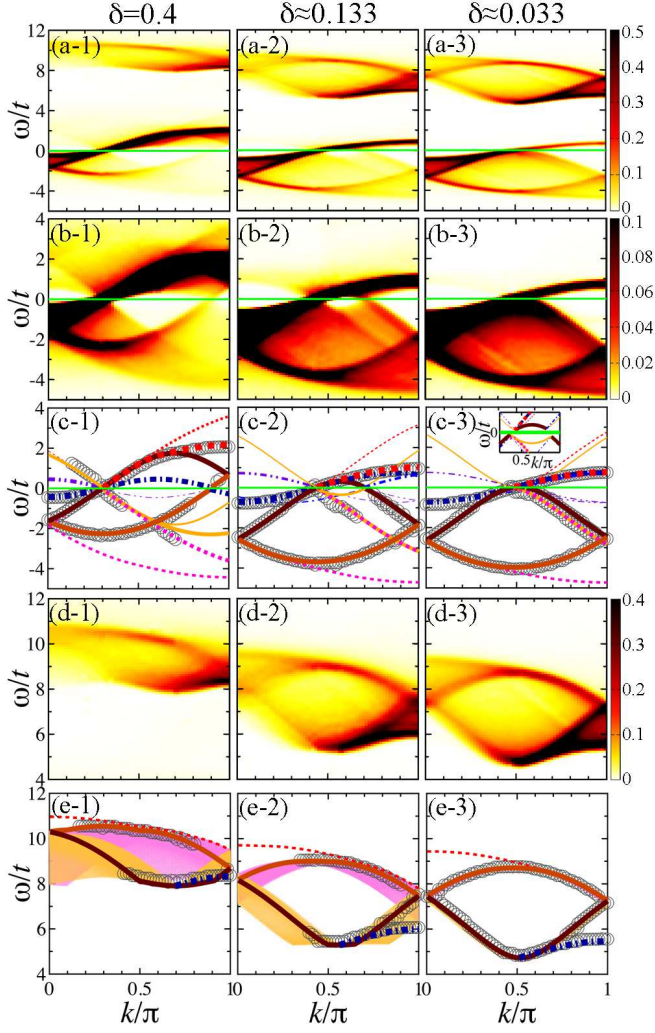


FIG. 2: (a,b,d)  $A(k, \omega)$  for  $U/t=8$  at  $\delta \approx 0.4, 0.133, 0.033$  (from the left) for (a) overall behaviors, (b) lower, and (d) upper Hubbard bands. (c,e) Dispersion relations obtained using the Bethe ansatz in  $L=240$ , corresponding to (b,d). Solid lines except green ones at  $\omega=0$  show holon and antiholon modes. Blue dashed-dotted lines denote spinon modes. Red (pink) dotted lines show upper (lower) edges of continua of  $hh^*$  with  $s(k_F)$  and  $h^*(2k_F)$ ,  $sh^*$ ,  $hh^*$  with  $s(k_F)$ , and  $shh^*$  (from above) in (c), and  $shd$  in (e). Purple dashed double-dotted lines in (c) denote spinon modes in 2- $\Lambda$ -string solutions. Open circles indicate peaks of dominant modes of (b,d). The inset in (c-3) is the closeup near the gapless points. The pink [yellow] region in (e) denotes the  $hd$  continuum with  $s(-k_F)$  [ $s(k_F)$ ]. Spinon [holon] modes in (e) have  $h(\pm 2k_F)$  and  $d(\pm(\pi - 2k_F))$  with  $q_d q_h > 0$  [ $s(\pm k_F)$  and  $d(|q_d| \approx \pi\delta/2, q_d q_h > 0)$ ].

identified as the  $h^*$  mode with  $s(k_F)$ . On the basis that the mode has charge character and that the momentum region between these two gapless points shrinks as  $\Delta k = 2\pi\delta$ , this region can be regarded as the hole pocket. It is naturally expected that the  $h^*$  mode will become robust as  $U/t$  increases because of the reduction in double occupancies. In fact, the  $h^*$  mode has been found for  $U/t \rightarrow \infty$  [8] and in the 1D  $t$ - $J$  model [13].

*Spectral-weight transfer.*— Although the spectral weight  $A$  transferred to LHB for  $\omega > 0$  equals the amount of doping ( $A = \delta$ ) at  $t = 0$  [14], Fig. 1(e) shows that  $A > \delta$  for  $t \neq 0$ . Such behaviors have been discussed in the literature [3, 14, 15]. [For  $\omega < 0$ ,  $A = (1 - \delta)/2$  as usual.] The question here is which mode carries the transferred spectral weight. As in Figs. 2(b-3) and (c-3), a considerable weight is carried by the mode of the upper edge of the  $sh^*$  continuum. In the  $\delta \rightarrow 0$  limit, where  $|q_{h^*}| \rightarrow \pi$ , this mode reduces to the  $s$  mode with  $h^*(\pm\pi)$ ; the dispersion relation  $\epsilon(k)$  is obtained as follows:

$$\epsilon = \frac{2t^2}{U} \int_{-\pi}^{\pi} dq \cos^2 q \operatorname{sech} \frac{2\pi t(\Lambda_s - \sin q)}{U}, \quad (1)$$

$$k = \frac{\pi}{2} + \frac{t}{U} \int_{\Lambda_s}^{\infty} dx \int_{-\pi}^{\pi} dq \operatorname{sech} \frac{2\pi t(x - \sin q)}{U},$$

using dressed energies and momenta for  $\delta \rightarrow 0$  [16, 17]. This gapless mode naturally leads to the 2-spinon continuum at half-filling expressed as  $E(k) = \epsilon(k_1) + \epsilon(k_2)$  with  $k = k_1 + k_2 - \pi$  [16, 17]: the two gapless modes carrying  $S=1/2$  with gapless points at  $k = \pm k_F$  cause the gapless  $S=1$  spin excitations with the gapless point at  $|k| = 2k_F$ . It should be noted that the cosine dispersion relation in the  $U/t \rightarrow 0$  limit as well as the flat dispersion relation in the  $U/t \rightarrow \infty$  limit [18] are reproduced, since  $\epsilon(k) \simeq -2t \cos k$  for  $U \ll t$  and  $\epsilon(k) \simeq -\frac{\pi J}{2} \cos k$  with  $J \equiv 4t^2/U$  for  $U \gg t$  [16] for  $|k \pm \pi| < \pi/2$ . This implies that the spectral weights transferred by infinitesimal doping spread up to the energy of  $O(t)$  for small  $U/t$  and  $O(J)$  for large  $U/t$ , as in Figs. 1(b-2,3,c,f) and 2(b-3). This behavior is contrasted with band-insulator-to-metal transitions, where the spectral weight transferred by doping is located within the energy range of the chemical potential shift of  $O(\delta^{2/D})$  for  $\delta \rightarrow 0$  in  $D$  dimensions.

*Upper Hubbard band.*— To identify the dominant modes in UHB, we consider the solutions with a  $k$ - $\Lambda$  string, i.e., a pair of complex  $k_j$ 's with a non-zero imaginary part, which represents a pair of electrons [12]. Since such solutions have energies of  $O(U)$  in the large  $U/t$  regime [12, 16], it is natural to expect that they are relevant for UHB [9, 19]. In fact, it has been found that solutions with a string length greater than one have considerable spectral weights in the high-energy regime for quasi-1D spin models [20, 21] and spinless-fermion chains [22, 23]. The  $k$ - $\Lambda$  string is characterized by a half-odd integer or an integer  $\bar{I}_1$ . We call the quasiparticle for the  $k$ - $\Lambda$  string doublon and denote it as  $d$ ; the momentum is defined as  $q_d = 2\pi\bar{I}_1/L$  in  $|q_d| < \pi - 2k_F = \pi\delta$  [12]. We define the sign of  $q_d$  such that  $k = -q_s - q_h + q_{h^*} - q_d$ .

At half-filling,  $A(k, \omega)$  of UHB is symmetric with that of LHB because of the particle-hole symmetry. In the small-doping regime,  $A(k, \omega)$  remains almost symmetrical, as in Figs. 1(f) and 2(a-3). In the  $\delta \rightarrow 0$  limit, where  $|q_d| \rightarrow 0$ , the dominant modes in UHB are characterized by  $s$  and  $h$  in the  $k$ - $\Lambda$ -string solutions, and have essentially the same character as that in LHB. Namely, the low-energy mode for  $k \gtrsim k_F \simeq \pi/2$  in Fig. 2(d-3)

is identified as the  $s$  mode with  $h(\pm 2k_F)$  and  $d(q_d \simeq 0)$ , as in Fig. 2(e-3). The mode slightly above it and the low-energy mode for  $k \lesssim k_F$  are both identified as the  $h$  mode with  $s(k_F)$  and  $d(q_d \simeq 0)$ . The high-energy mode is identified as the  $h$  mode with  $s(-k_F)$  and  $d(q_d \simeq 0)$ , which corresponds to the shadow band. For larger doping, the dominant modes with charge character in Fig. 2(d) remain within the  $hd$  continua with  $s(\pm k_F)$  [yellow and pink regions in Fig. 2(e)], and appear to have  $d(|q_d| \simeq \pi\delta/2, q_d q_h > 0)$  [solid lines in Fig. 2(e)].

*Discussion.*— To obtain an intuitive understanding of Mott transitions, two scenarios have been considered. One is that the effective carrier density ( $n^*$ ) vanishes, as in the case of metal-to-band-insulator transitions. The other is the effective-mass ( $m^*$ ) divergence in the Fermi liquid theory. The present results show that spectral weights are mainly transferred to the  $h^*$  mode with  $s(k_F)$  and the mode of the upper edge of the  $sh^*$  continuum [Figs. 1(b,c)]. The former behaves like  $n^* \rightarrow 0$ , because the hole pocket shrinks as  $\delta \rightarrow 0$ . The latter may seem to behave as  $m^* \rightarrow \infty$ , because its spectral weight decreases [Fig. 1(e)]. However, in a Fermi liquid, the width of the renormalized band near the chemical potential shrinks as  $\epsilon(k) \propto 1/m^*$  for  $m^* \rightarrow \infty$ , which is not the case for the present results wherein  $\epsilon(k)$  in Eq. (1) remains  $O(t)$  or  $O(J)$  [Fig. 1(c)]. Thus, a simple classification of  $n^* \rightarrow 0$  or  $m^* \rightarrow \infty$  is not accurate for the Mott transition of the Hubbard chain; the Mott transition is rather characterized as a loss of charge character from the mode having both spin and charge characters, while the dispersion relation of the spin part remains gapless and dispersing.

The nature of the Mott transition in the Hubbard chain may be more clearly understood through comparisons with the results of a recent cellular dynamical mean-field study on the Mott transition of the 2D Hubbard model in Ref. [3], where the following features have been discussed. (1) The phase transition from a large Fermi surface to hole pockets occurs at nonzero  $\delta$ . (2) The transferred spectral weight behaves as  $A = \delta + \langle n_{i\uparrow} n_{i\downarrow} \rangle$  after tiny doping  $\delta \lesssim 0.01$ . (3) A gap fully opens between the band of hole pockets and that of ingap states for  $\omega > 0$  below UHB, leading to the zero surface of the Green function. (4) The pseudogap can be attributed to doublon (doubly occupied site)-holon (empty site) binding relaxed due to doping.

In contrast, for the Hubbard chain, (1) there is no phase transition when  $\delta \neq 0$ : the gapless point at  $k = 2\pi - 3k_F$  persists even in the large doping regime, where the gapless point goes beyond the zone boundary ( $k = \pi$ ) and is located at  $k = 3k_F$ , as in Fig. 2(b-1). (2) The transferred spectral weight does not follow  $A = \delta + \langle n_{i\uparrow} n_{i\downarrow} \rangle$ , and gradually reaches zero as  $\delta \rightarrow 0$ , as in Fig. 1(e). (3) The cosine-like mode and the antiholon mode are both gapless at  $k = k_F$ : there is no gap between them at  $k = k_F$ . The gapless cosine-like mode is related to the gapless spin excitations. (4) Double occupancy in

LHB does not behave as a quasiparticle. The quasiparticle for a pair of electrons is defined in the  $k$ - $\Lambda$ -string solutions, which are relevant only for UHB: the pseudogap behavior in LHB is not related to the quasiparticle. Understanding and explaining the above differences can be an interesting topic for future study.

*Summary.*— The single-particle spectral properties near the Mott transition were investigated using the Bethe ansatz and DDMRG method in the 1D Hubbard model. By identifying the dominant modes, characteristic spectral features near the Mott transition, such as the pseudogap, hole-pocket behavior, spectral-weight transfer, and upper Hubbard band, were explained in a unified manner in terms of spinons, holons, antiholons, and doublons. A remarkable feature is the emergence of the gapless mode extending up to  $O(t)$  [ $O(J)$ ] for small [large]  $U/t$  by infinitesimal doping. This mode is related to the spin excitations at half-filling, and cannot be interpreted by either the rigid-band picture or the Fermi liquid theory. The present results have similarities to the anomalous spectral features observed in high- $T_c$  cuprates [1, 2] and some aspects of the 2D Hubbard model [3, 15, 24]. I expect that generic features of Mott transitions in finite dimensions can be deduced from the present results.

I am grateful to S. Fujimoto and M. Arikawa for discussions. This work was supported by World Premier International Research Center Initiative on Materials Nanoarchitectonics, MEXT, Japan, and KAKENHI 22014015.

---

- [1] A. Damascelli *et al.*, Rev. Mod. Phys. **75**, 473 (2003).
- [2] J. Meng *et al.*, Nature (London) **462**, 335 (2009).
- [3] S. Sakai *et al.*, Phys. Rev. Lett. **102**, 056404 (2009).
- [4] E. Jeckelmann, Phys. Rev. B **66**, 045114 (2002).
- [5] E. Lieb and F.Y. Wu, Phys. Rev. Lett. **20**, 1445 (1968).
- [6] H. Benthien *et al.*, Phys. Rev. Lett. **92**, 256401 (2004).
- [7] H.J. Schulz, in *Correlated Electron Systems*, edited by V.J. Emery (World Scientific, Singapore, 1993), p. 199.
- [8] K. Penc *et al.*, Phys. Rev. Lett. **77**, 1390 (1996).
- [9] H. Benthien, Ph.D. thesis, Marburg, 2005.
- [10] H.J. Schulz, Phys. Rev. Lett. **64**, 2831 (1990).
- [11] R. Preuss *et al.*, Phys. Rev. Lett. **73**, 732 (1994).
- [12] M. Takahashi, Prog. Theor. Phys. **47**, 69 (1972).
- [13] C. Lavalle *et al.*, Phys. Rev. Lett. **90**, 216401 (2003).
- [14] H. Eskes *et al.*, Phys. Rev. Lett. **67**, 1035 (1991).
- [15] P. Phillips, Rev. Mod. Phys. **82**, 1719 (2010).
- [16] M. Takahashi, *Thermodynamics of One-dimensional Solvable Models* (Cambridge University Press, 1999).
- [17] F.H.L. Essler *et al.*, *The One-Dimensional Hubbard Model* (Cambridge University Press, 2005).
- [18] J. Favand *et al.*, Phys. Rev. B **55**, R4859 (1997).
- [19] F. Woynarovich, J. Phys. C **15**, 85 (1982).
- [20] M. Kohno, Phys. Rev. Lett. **102**, 037203 (2009).
- [21] M. Kohno, Phys. Rev. Lett. **103**, 197203 (2009).
- [22] M. Kohno *et al.*, J. Phys. Soc. Jpn. **79**, 043707 (2010).
- [23] R.G. Pereira *et al.*, Phys. Rev. B **79**, 165113 (2009).
- [24] T.D. Stanescu *et al.*, Phys. Rev. B **74**, 125110 (2006).